Surface & Coatings Technology 321 (2017) 292–299

Contents lists available at ScienceDirect

Surface & Coatings Technology

journal homepage: www.elsevier.com/locate/surfcoat

The influence of thermal annealing on the structural, optical and electrical properties of AZO thin films deposited by magnetron sputtering

Daniel Meljanac [a,*], Krunoslav Juraić [a], Vilko Mandić [b], Hrvoje Skenderović [c], Sigrid Bernstorff [d], Jasper R. Plaisier [d], Ana Šantić [a], Andreja Gajović [a], Branko Šantić [a], Davor Gracin [a]

[a] Ruđer Bošković Institute, Bijenička 54, HR-10000 Zagreb, Croatia
[b] University of Valenciennes and Hainaut-Cambresis, Boulevard du General de Gaulle, FR-59600 Maubeuge, France
[c] Institute of Physics, Bijenička 46, HR-10000 Zagreb, Croatia
[d] Elettra-Sincrotrone Trieste, SS 14, Km 163.5, I-34049 Basovizza, (TS), Italy

ARTICLE INFO

Article history:
Received 16 March 2017
Revised 20 April 2017
Accepted in revised form 27 April 2017
Available online 28 April 2017

Keywords:
Al-doped zinc oxide
Hydrogen atmosphere
Transparent conducting oxide
Magnetron sputtering
Conductivity
Point defects

ABSTRACT

Thin Al-doped ZnO (AZO) films were deposited by magnetron sputtering on a non-heated quartz substrate. As-deposited samples have a nanocrystalline structure, a high transparency in the visible part of the spectrum, but a relatively low conductivity. After deposition, the films were isochronally annealed for one hour in hydrogen atmosphere at 200, 300 or 400 °C. The influence of such treatment on the structural properties was analysed by GIXRD and correlated with UV–Vis, photoluminescence and impedance measurements.

The structural investigation demonstrated that the heat treatment reduces the strain in the material, the volume of the crystal lattice decreases and the crystal size grows. By measuring the optical properties it was shown that heating increases the optical gap and gradually reduces the number of point defects, mostly related to interstitial atoms. As a result of this process, the conductivity at room temperature increased >9 orders of magnitude due to an enhancement of the mobility and the concentration of free carriers.

The activation energy for defect annihilation was estimated to be about 1 eV and corresponds to the diffusion of interstitial atoms with the annihilation of vacancies. The concentration of free carriers increases due to the activation of the dopants that act as shallow donors.

1. Introduction

Zinc oxide is a material which is suitable for many applications due to the large band gap (3.37 eV), high carrier mobility, and a relatively high exciton binding energy (60 meV). The luminescence in UV, blue, green, yellow and red makes ZnO interesting for various applications in optical devices and optoelectronics [1–6]. The combination of high conductivity and transparency for visible light nominates this material as a possible candidate for front electrodes, as a transparent conductive oxide (TCO) in thin film solar cells. Additionally, it is possible to produce ZnO in a variety of nanostructured forms with large actual to nominal surface ratio [7], which helps the light harvesting and leads to higher efficiency.

For the use as a conductive layer, ZnO is typically doped with Al or Ga, which act as shallow donors. Although ZnO has been extensively studied because of these interesting optical and electrical properties, the origin of the *n*-type conductivity has not yet been fully understood. Since these properties are largely affected by defects and impurities, it is of great importance to better understand the role of defects regarding the conductivity of ZnO. The most relevant defect among the point defects in intrinsic ZnO is probably the zinc vacancy (V_{Zn}). It has the lowest formation energy among native point defects in *n*-type ZnO [8], and it is suggested that it forms complexes with donors limiting their doping activity [9]. Furthermore, one of the limiting factors for achieving minimum resistivity in aluminium doped ZnO thin films appears to be the deactivation of the Al dopant by a vacancy-type defect.

Besides the practical application possibilities, photoluminescence (PL) is a great tool to detect and identify the energy levels of the defects in a material. A lack of photoluminescence indicates a high concentration of defects that act as non-radiative recombination centres. PL of ZnO has been extensively investigated, but in the case of nanostructured thin films, there is still a controversy regarding the attribution of certain PL peaks to specific types of defects. Namely, due to the high surface-to-volume ratio on the nanometre scale, the surface defects play an important role for the optoelectronic properties [5]. That is why every film growth method results in different types of defects and/or defect complexes, located on different energy levels inside the band gap.

ZnO films can be deposited in many ways using chemical and physical techniques. Although the growth and properties of ZnO

* Corresponding author.
E-mail address: dmeljan@irb.hr (D. Meljanac).

http://dx.doi.org/10.1016/j.surfcoat.2017.04.072
0257-8972/

nanostructures have been extensively studied [10], there are still a number of unanswered questions concerning the relationship between details of the fabrication conditions and the optical properties. For the application purposes, it is also important to have a deposition method that is reproducible and can be easily up scaled for industrial use. In this sense, magnetron sputtering has a number of advantages, such as high deposition rate and ease of automation. Furthermore, sputtering can be combined with post-deposition annealing, which can modify and improve the properties of various metal oxides [11–13].

In this study, we explore the possibility to improve the electrical properties of AZO thin films by heat treatment in hydrogen atmosphere. It was reported that a post-deposition heat treatment could improve the quality of the film properties, i.e. reduce stress in the films and improve their crystallinity [14]. Also, for similar AZO layers prepared at room temperature, subsequent annealing at a higher temperature can produce different effects depending on the annealing atmosphere. In the case of oxygen and nitrogen atmosphere, the AZO samples exhibited poor crystallinity and high resistivity [15]. On the other hand, thermal treatment in hydrogen atmosphere could improve the electrical properties, and possibly increase the optical transmission [16–18]. Since the heating was done in hydrogen atmosphere, we also expected a positive role of hydrogen in improving the electrical conductivity, due to the removal of oxygen species absorbed in the films, which should result in an increase of the carrier mobility.

That is why we investigate the role of defects on the conductivity of AZO films by applying post-deposition heat treatment in hydrogen atmosphere. The films were deposited by DC magnetron sputtering of ZnO:Al on a non-heated quartz substrate. The deposition was performed at room temperature, expecting that in this way many defects will be created in the films, so that the influence of the post-deposition thermal treatment in hydrogen atmosphere will be more evident. After deposition, the samples were heated for one hour in a hydrogen atmosphere at temperatures of 200, 300 or 400 °C.

First, we investigated the effect of heating in hydrogen atmosphere on the structural and optical properties of AZO thin films, and then the electrical properties were studied. The nanostructural changes were analysed by Grazing Incidence X-ray Diffraction (GIXRD), while the electrical and dielectric properties were investigated by impedance spectroscopy. Information about the point defects dynamic was obtained by luminescence measurements.

2. Material and methods

2.1. Sample preparation

Aluminium doped zinc oxide (AZO) thin films were deposited on a non-heated quartz substrate by DC magnetron sputtering using a ceramic ZnO cathode with 3% of Al as a target. The base pressure and Ar gas pressure during deposition were $5 \cdot 10^{-5}$ Pa and 1.5 Pa, respectively. Sample 0 is the raw as-deposited AZO sample, while samples 1, 2 and 3 were subjected to heat treatment in hydrogen, with a duration of 1 h at 200, 300 or 400 °C, respectively. The film thickness was 700 nm.

2.2. Characterisation methods

The GIXRD experiment was done at the MCX beamline at the synchrotron Elettra (Trieste, Italy) [19,20]. The energy of the synchrotron radiation was 8 keV (1.55 Å). The angle of grazing incidence was set to 1° and kept constant during the single 2θ scan. The corresponding penetration depth for bulk ZnO of 600 nm ensures to probe the entire layer from the surface to the substrate. The scanned 2θ range was (20°–80°) with a step size of 0.02°.

An UV–Vis transmittance experiment was performed using a Xe 150 W light source and an Ocean Optics HR4000 spectrometer. From the obtained transmittance, the layer thickness and dielectric constants (index of refraction and extinction) were calculated using a point-wise unconstrained optimization approach, and approximating the sample geometry with one thin film layer with plan-parallel boundaries on a thick low-absorbing substrate, as described previously [21,22].

An impedance analyser (Novocontrol Alpha-AN Dielectric Spectrometer) was used to perform electrical and dielectric measurements [23] in the frequency range from 0.01 Hz to 1 MHz at a voltage of 10 mV and over a temperature range between 303 and 423 (±0.5) K in heating and cooling. The scan at each temperature was repeated twice. A Sputter Coater SC7620 was used to sputter two parallel thin film gold stripes (1 × 4 mm), distanced 4 mm using a template on the AZO thin films, to serve as electrodes. For the impedance spectroscopy (IS), platinum contact wires were fixed on the electrodes using a silver paste. The activation energy for dc conductivity, E_{dc}, for each sample was determined by Arrhenius plots from the slope of $\log\sigma_{dc}$ vs. $1 / T$ using the equation $\log\sigma_{dc} = \sigma_0 \exp(-E_{dc} / k_B T)$, where σ_{dc} is the dc conductivity, σ_0 is the pre-exponent, k_B is the Boltzmann constant and T is the temperature (K).

Photoluminescence (PL) measurements were performed with the fourth harmonic (wavelength 263 nm) of a pulsed Nd:YLF laser at 1 kHz repetition rate, and with 100 ns pulse duration and average power of 10 mW. The laser beam was mildly focused onto the sample resulting in a 100 μm diameter spot, which was imaged onto the entrance slit of a spectrograph (Shamrock 303i). After dispersion on a 150 grooves/mm grating the PL spectra were recorded by a thermoelectrically cooled CCD camera (AndoriDus). Each PL spectrum was taken with 1 s exposure time, and then averaged over 10 exposures [24].

3. Results and discussion

3.1. Structure

GIXRD diffraction patterns from the as-deposited AZO sample, and from samples annealed 1 h at 200, 300 or 400 °C, respectively, are shown in Fig. 1. The patterns of all as-deposited and treated AZO samples (Fig. 1) were assigned to zincite (ICDD PDF#36-1451) with hexagonal, wurzite crystal structure of the *P63mc* space group. Even though high preferential orientation is typical for deposited zincite thin films, the intensities ratio suggests the presence of an only low-to-moderate preferential orientation. For the as-deposited film (Sample 0) the diffraction peaks are quite broad, suggesting nanosized crystallites. During thermal treatment the peaks get narrower, which indicates a thermally activated process of grain growth. In order to monitor the influence of the thermal treatment on the structural and microstructural parameters (unit cell parameters, crystallite size and microstrain), all diffractograms were refined using the Rietveld method. Rietveld refinements of GIXRD spectra were carried out using starting parameters from the zincite structural model (ICSD #82028).

The obtained results (Table 1) show that the average crystallite size increased after heating of the samples from 9.7 nm for the as-deposited sample, to 17.2 nm for the sample heated at 400 °C. The observed phenomena are graphically presented in Fig. 2. Furthermore, the initial microstrain decreases after the heat treatment. Also, the parameters of the unit cell decrease gradually (Table 1).

3.2. Optical properties

The structural changes are reflected also in the changes of the optical properties. The dependence of the optical properties on the annealing temperature was investigated by measuring the transmittance in the visible part of the spectrum. Transmittances of the as-deposited and the hydrogen annealed AZO films are shown in Fig. 3, in the wavelength range of 300–800 nm. As shown in the figure, the samples are transparent in the visible part of the spectrum. It is apparent that the absorption edge moves towards shorter wavelengths with increasing annealing temperature for the AZO samples. This means that the transmittance

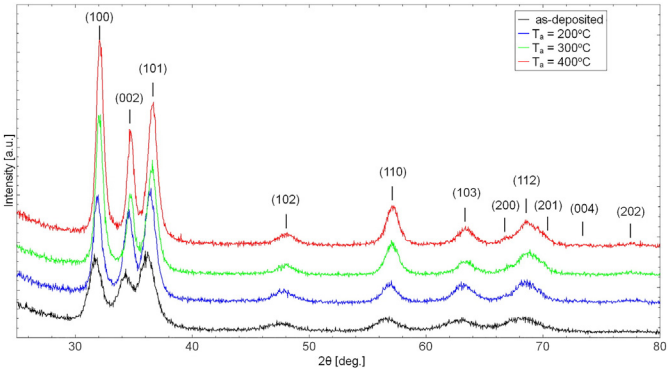

Fig. 1. GIXRD patterns of magnetron sputtered AZO thin films: as-deposited and annealed at 200, 300 or 400 °C, assigned to zincite (ICDD PDF#36-1451); the Miller indices are denoted above the diffraction peaks.

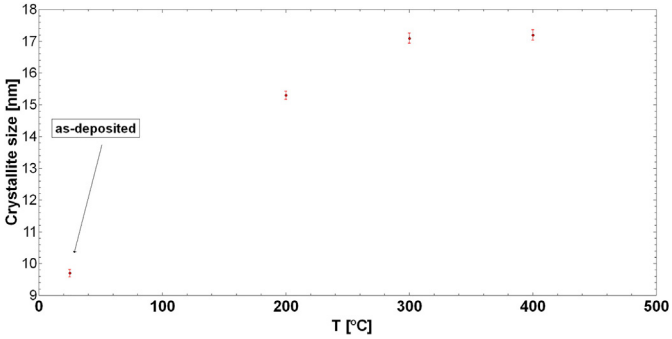

Fig. 2. Crystallite size as a function of annealing temperature.

increased, i.e. the energy gap increased. The blueshift of the absorption edge with increasing annealing temperature up to 400 °C is attributed to the Burnstein-Moss effect [25]. This bandgap energy (Eg) broadening is caused by an increased free electron concentration due to the Al doping. Eg can be deduced from the Tauc plot [26].

From Fig. 4, it is evident that, as expected, the absorption coefficient, α, obeys the Tauc relation:

$$(\alpha h\nu)^{1/2} = A\,(h\nu - Eg) \quad (1)$$

where A is a constant, hν is the energy of the incoming light, and Eg represents the Tauc optical gap [27]. The determined Eg of as deposited samples was around 2.85 eV and increased gradually up to 3 eV after annealing in hydrogen atmosphere (Fig. 5).

3.3. Photoluminescence

The effect of the thermal treatment on the defect dynamics in the MS AZO thin films deposited at room temperature can be well monitored by photoluminescence (PL) measurements. The relation of different PL bands and the origin of the defects were extensively studied in the known literature. The dominant bulk defect should be singly ionized zinc vacancies, V_{Zn}^{-}, acting as shallow acceptors [28]. This is in agreement with theoretical calculations [29], which ascribe the blue luminescence to Zn vacancies. Also, in some other experiments, the peak around 3 eV is attributed to Zn vacancies [24,30]. The red luminescence is mostly attributed to oxygen interstitials, O_i [31–33].

In Fig. 6 is shown that the as-deposited sample does not have well defined PL intensity peaks. There are 2 broad bands, around 3.2 eV (UV) and 2.6 eV (blue). The UV band is attributed to a band to band transition, while the others are defect related.

In ZnO, the possible intrinsic defect centres are (i) zinc vacancies (V_{Zn}), (ii) zinc on interstitial sites (Zn_i), (iii) oxygen on interstitial sites (O_i), and (iv) oxygen vacancies (V_O). The extrinsic defect in our samples appeared due to the Al dopant which is a shallow donor in ZnO and introduces an additional level close to the conduction band. This level could shift and broaden the luminescence peaks.

As seen from Fig. 6, heating the sample to higher temperatures during the thermal treatment in hydrogen atmosphere resulted in a change of the UV to defect bands ratio. For the as-deposited AZO sample, the PL spectrum shows that the UV peak has a slightly larger intensity than the blue peak. By heating the sample at 200 °C, the photoluminescence almost disappears, which means that the defects start to move and rearrange inside the lattice. This indicates the formation of non-radiative recombination centres. At the higher temperature of 300 °C the photoluminescence related with defects reappears. The defect related peaks at 2.4 and 2.75 eV dominate at this temperature, including a new broad PL peak at 1.9 eV (red) attributed to oxygen interstitial atoms, O_i. At 400 °C we get two well defined peaks: in the UV (3.19 eV) and also a blue peak (2.62 eV). The blue peak is attributed to zinc vacancies, V_{Zn}. Also, the UV peak is now narrower and more intense, so the difference between the blue peaks is substantial. This observation indicates a lower density of Zn vacancies. Furthermore, the luminescence peak related to the band-to-band transition (UV peak) is narrower and better defined, indicating an improvement of the crystal structure, which is consistent with a decreasing density of bulk defects. The peak in the red region (1.9 eV) has vanished. Since the heat treatment was done in a hydrogen atmosphere, the surface oxygen interstitial atoms most probably formed bonds with hydrogen and disappeared from the surface.

It is obvious that the PL intensity of the AZO films heated in hydrogen atmosphere at 400 °C is stronger than that of the as-deposited film. The strong PL intensity of the AZO films heated in a hydrogen atmosphere is considered to be due to the removal of defects that acted as non-radiative recombination centres on grain boundaries. It is well known [34] that in the case of ZnO, the negatively charged oxygen interstitial ions that are absorbed on the surface of grain boundaries decrease the PL peak intensity by binding with photogenerated holes. These oxygen ions can be removed from the ZnO surface with thermal treatment in hydrogen atmosphere [34].

Table 1
The unit cell parameters of all as-deposited and annealed samples, and their microstrain.

Sample no.	T [°C] annealing temperature in H_2	a [Å]	c [Å]	e [$\times 10^4$] strain
0	as-deposited	3.255	5.240	175
1	200	3.254	5.215	123
2	300	3.250	5.207	104
3	400	3.250	5.201	98

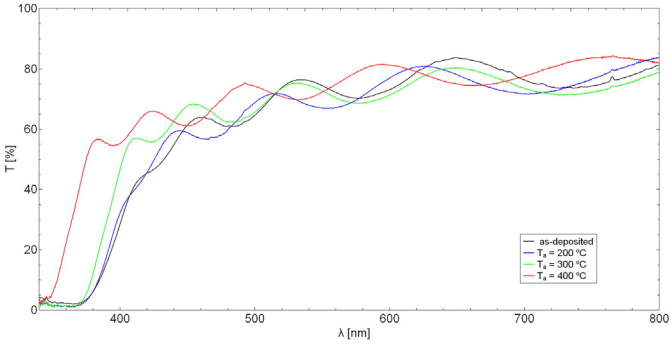

Fig. 3. Transmittance spectra of the as-deposited and hydrogen-annealed AZO thin films on quartz substrate at three temperatures: 200, 300 and 400 °C.

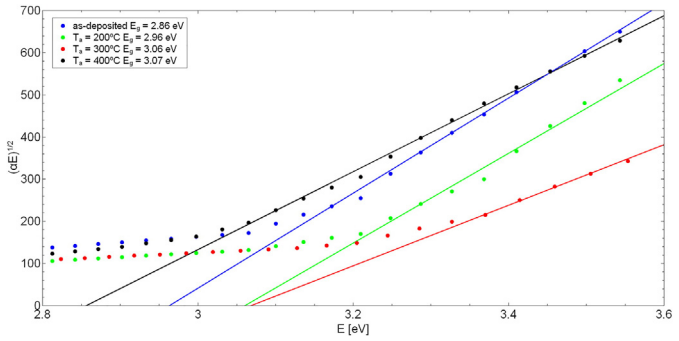

Fig. 4. Mathematical fit to the Tauc relation (Eq. 1).

3.4. Impedance spectroscopy analysis

Impedance spectroscopy measurements were performed in the temperature range from 30 to 150 °C in heating and cooling cycles. Fig. 7. shows the sheet conductivity spectra at different temperatures for all AZO thin films recorded during a cooling cycle. The as-deposited AZO thin film (sample 0) exhibits the lowest sheet conductivity, while the conductivity increases drastically with annealing temperature.

Moreover, there is an obvious difference in the frequency dependence of the sheet conductivity between the as-deposited and annealed AZO thin films. While the latter show frequency independent conductivity in the whole experimental frequency range, i.e. dc sheet conductivity (σ_{dc}), the as-deposited sample exhibits a frequency-dependent region. The frequency-independent plateau at low frequencies in case of the as-deposited sample is attributed to the long-range translational motion of charge carriers and corresponds to the dc sheet conductivity; whereas with increasing frequency, the conductivity increases giving rise to an additional frequency-independent plateau. Such behaviour indicates two contributions to the electrical response of the as-deposited AZO thin film, most probably related to crystalline grains, and an electrically more resistive grain boundary [35].

The two contributions are also reflected in the shape of the impedance complex plane of as-deposited AZO, where a barely visible semicircle is present at the highest frequencies (see Fig. 8a). In contrast, the complex impedance plots for the thin film annealed at 200 °C clearly show only one semicircle at each temperature confirming the single conduction mechanism in this sample (Fig. 8b).

The impedance semicircles for as-deposited AZO thin film are poorly resolved and their separation is difficult. On the other hand, a much

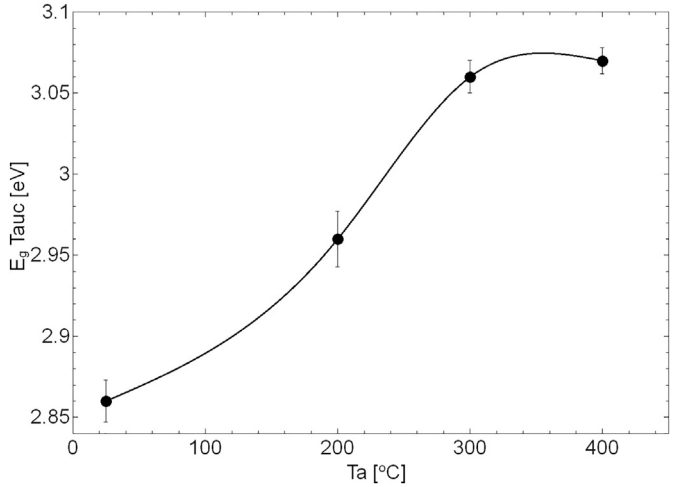

Fig. 5. Tauc optical gap as a function of annealing temperature.

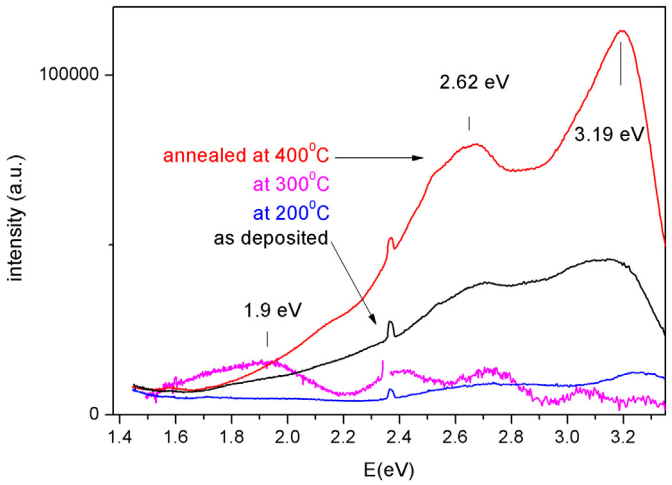

Fig. 6. PL spectra of the AZO thin films deposited by magnetron sputtering and thermally treated in hydrogen atmosphere. (For interpretation of the references to color in this figure, the reader is referred to the online version of this chapter.)

better resolution of the two contributions is visible in the complex electrical modulus function [36].

The complex electrical modulus, M^*, is related to the complex impedance, Z^*, by the relation: $M^* = i\omega C_0 Z^* = M' + iM''$, where C_0 is the vacuum capacitance of the empty measuring cell. The frequency dependence of the imaginary part of the electrical modulus is shown in Fig. 9.

The two well-defined M'' peaks for as deposited AZO sample are related to two electrical relaxations; the low-frequency peak is associated to the grain boundary contribution, whereas the high frequency peak originates from the bulk (grain) response. As expected, the single M'' peak for the annealed sample indicates the absence of any grain boundary contribution.

Each M'' peak is related to the characteristic relaxation time (τ_σ) which can be extracted from the position of the M'' maximum via the relation indicated in Fig. 9. For the as-deposited sample, the maxima in the M'' peaks shift to higher frequencies with increasing temperature, indicating that both relaxation processes are thermally activated. The plot of the relaxation frequency, $f_{M''}$, versus $1/T$ is represented by an Arrhenius equation, $f_{M''} = f_{0M''}\exp(-E_{M''}/kT)$, where $E_{M''}$ is the activation energy for the electrical relaxation, Fig. 10.

The onset of a frequency dependent region, which shifts towards higher frequencies with increasing annealing temperature, suggests a

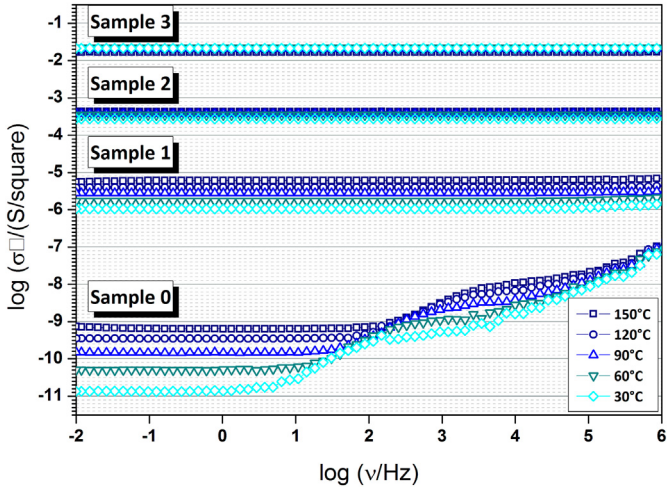

Fig. 7. Frequency dependence of the ac sheet conductivity at different temperatures for the AZO samples annealed in hydrogen atmosphere.

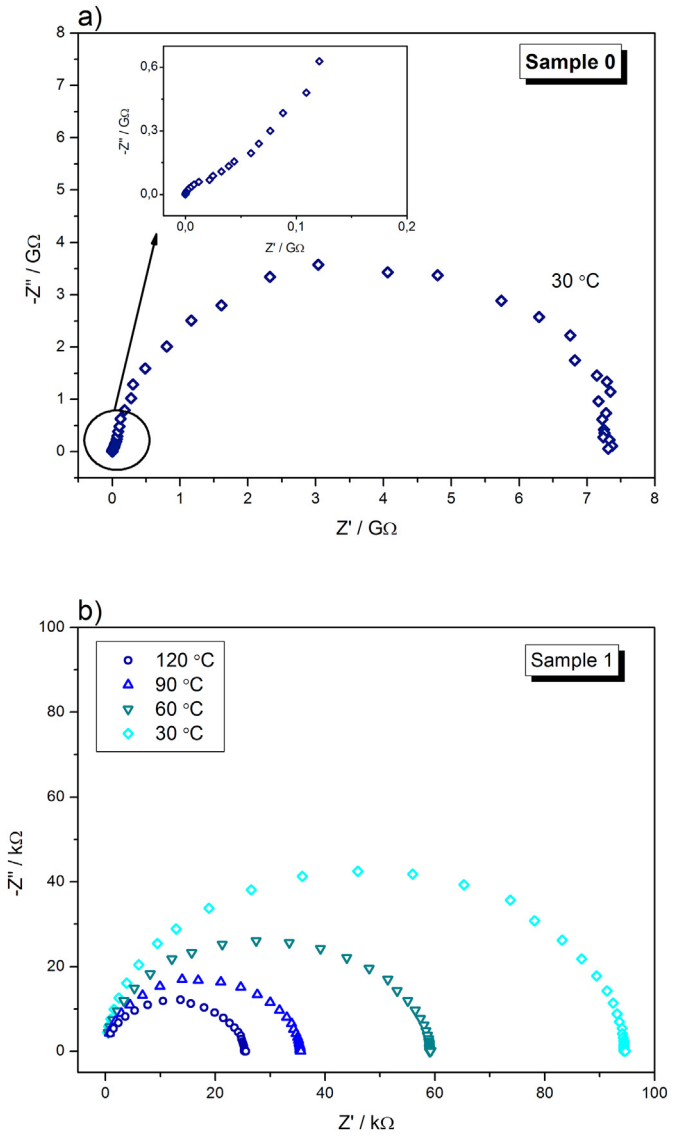

Fig. 8. Complex impedance plots for the as-deposited and the AZO thin film annealed at 200 °C; a) sample 0, b) sample 1.

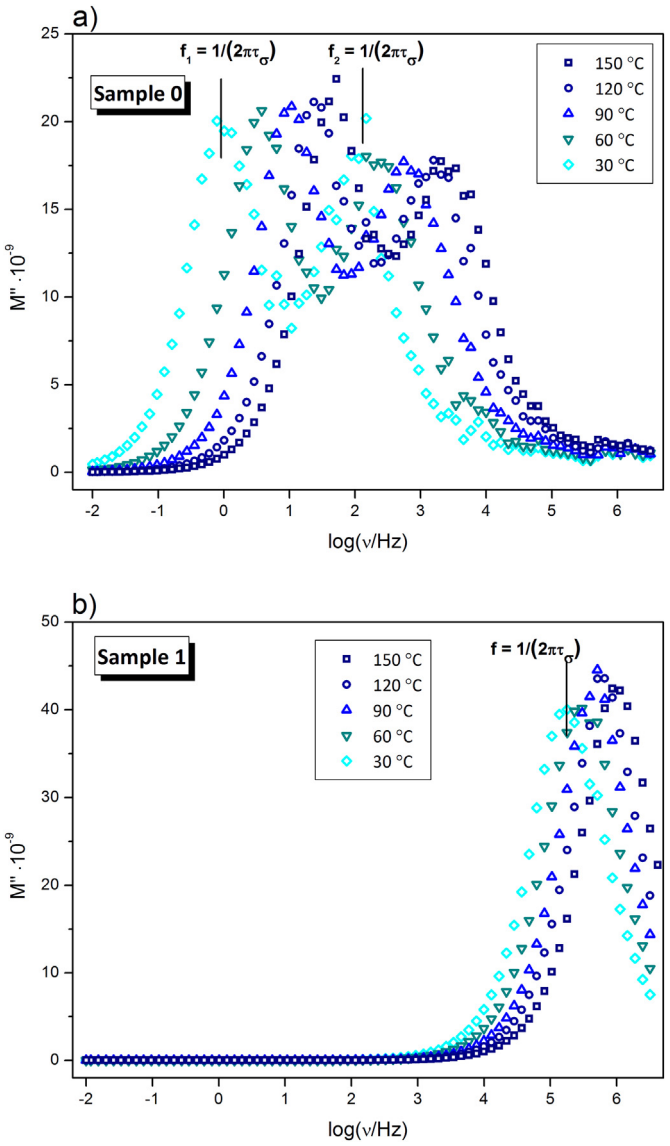

Fig. 9. Imaginary part of the complex electrical modulus as a function of frequency and temperature for the as-deposited and the AZO thin film annealed at 200 °C; a) sample 0, b) sample 1.

mobility increase of the carriers in the lattice [37]. Such behaviour was observed in the literature by surface sensitive characterisation methods (like XPS). Our results obtained with the IS method suggest that such behaviour appears in the bulk of the samples as well.

The activation energy for the relaxation in the bulk is 0.31 eV, whereas a slightly higher value of 0.37 eV, assigned to the grain boundary, indicates slower conduction processes and, hence, a less conductive phase. The obtained values are very similar to those of the grain and grain boundary conduction in non-doped nanophase ZnO (≈0.29 eV) as reported by Jose and Khadar [38,39]. It is interesting to note that the difference in the activation energy between grain and grain boundary is not large suggesting that both phases are similarly low-conducting, most probably due to a large number of point defects, mainly zinc vacancies, in both. Nevertheless, a slower relaxation associated to the grain boundary implies that this phase is structurally more defective and has a blocking effect on the electronic transport. All annealed AZO samples exhibit a single conduction process, excluding the contribution of the grain boundary, and a huge increase in the sheet conductivity with increasing annealing temperatures, Fig. 7. Also, the thermal activation of the sheet conductivity strongly changes with annealing. For the as-deposited sample the sheet conductivity values increases for two orders of magnitude in the temperature range 30–150 °C, while this increase becomes smaller for samples annealed at 200 and 300 °C. The sample annealed at 400 °C shows even the opposite behaviour, i.e. a decrease in the conductivity with increasing temperature. The activation energies for dc sheet conductivity, E_{dc}, for all samples were determined and presented in Fig. 11. Here, it should be noted that for the as-deposited sample the values of the dc sheet conductivity were read off from the low-frequency plateau in the conductivity spectra, which corresponds to the overall microscopic conductivity of the sample. The activation energy E_{dc} is the highest for the as-deposited sample with a value of 0.357 eV. This can be considered as the average value, yet it is very close to the activation energy for the relaxation process at the grain boundary (Fig. 10), implying that the more resistive blocking grain boundary plays a dominant role in the electrical transport in this sample. Further, the activation energy drastically reduces to 0.160 eV and 0.029 eV for the samples annealed at 200 and 300 °C, respectively. Obviously, the thermal treatment in hydrogen highly facilities the charge transfer mobility and thus significantly increases the dc sheet conductivity. For the sample annealed at 400 °C even a metallic behaviour occurred.

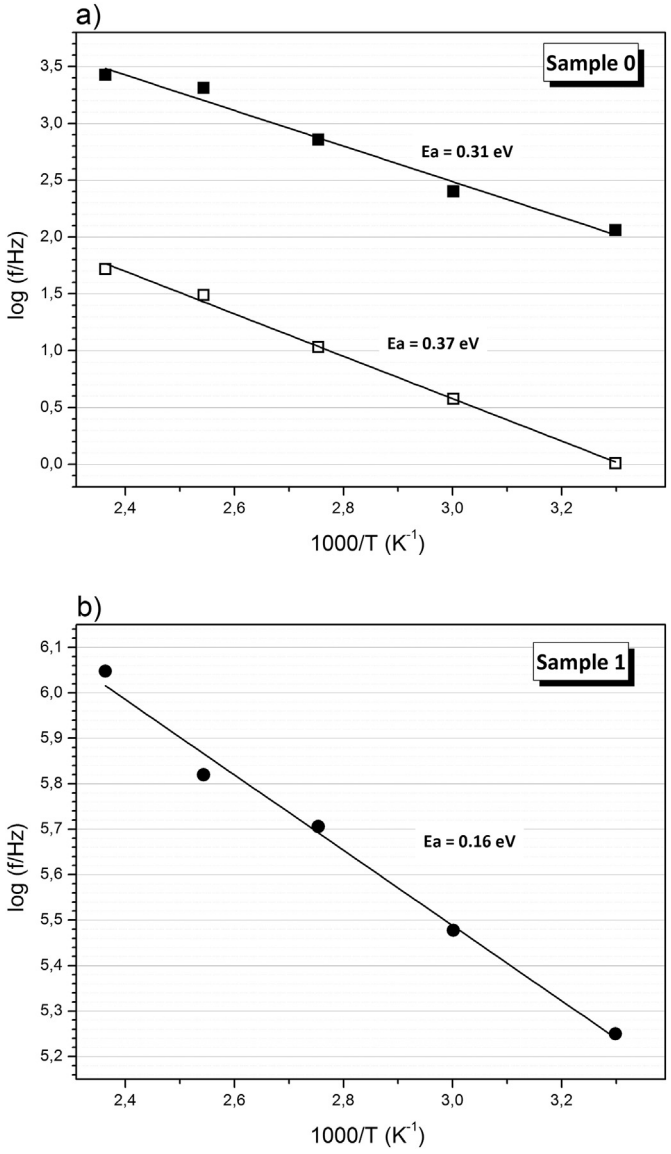

Fig. 10. Temperature dependence of the relaxation frequencies $f_{M''}$ for a) the as deposited sample 0, showing two relaxations; and b) sample 1showing only a single relaxation.

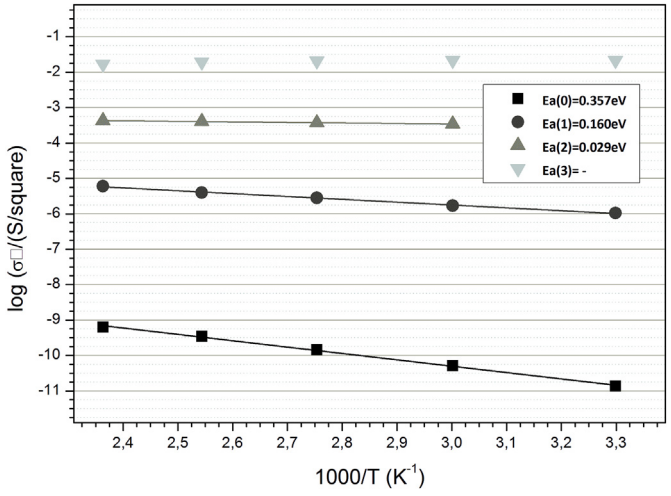

Fig. 11. Activation energies for dc sheet conductivity, E_{dc}, for the as-deposited sample 0 and the annealed AZO thin film samples 1, 2 and 3.

4. Discussion

The results for the specific DC resistivity measured at room temperature after annealing are shown in Fig. 12 as a function of the annealing temperature. From the figure, an exponential change of the resistivity with annealing temperature can be observed. The exponential function describing thermally activated processes with the required activation energy in the order of 1 eV fits the data well. Most probably, there are several parallel processes that result in an increase of the conductivity. A drastic increase in the sheet conductivity and a decrease in the activation energy with increasing annealing temperature can be mainly attributed to the annihilation of defects. This activates the Al donor atoms and thus leads to an increase of the free carrier concentration. The most likely effects of thermal treatment that correspond to the observed activation energy are recombination of close interstitial-vacancy pairs and free migration of interstitial atoms and vacancies. The characteristic energy barriers for the migration of typical defects in monocrystalline ZnO are: ~1.4 eV for zinc vacancies (V_{Zn}), ~2.4 eV for oxygen vacancies (V_O) in the *n*-type material, ~0.5 eV for zinc interstitials (Zn_i), and ~1 eV for oxygen interstitials (O_i) [40,41]. Hence, the movement of interstitial atoms requires the least energy. Therefore, one of the dominant processes that occur in our samples during the thermal treatment is most probably the annihilation of vacancies with atoms which are on interstitial positions in the as-deposited films. This is consistent with the observed annealing induced reduction of the unit cell parameters (Table 1). The PL intensity of the blue peak, related to the zinc vacancies defects in our measurements, is reduced by heating (Fig. 6), which confirms this attribution and agrees well with the GIXRD results. Also the PL peak at 1.9 eV, which is attributed to interstitial oxygen atoms, disappears with annealing (at 400 °C), which is in accordance with the above mentioned assumptions about the dominant processes during annealing. Furthermore, from IS it is also concluded that the as-deposited AZO thin film shows contributions of crystalline grains and grain boundaries in the electrical response. As for all annealed AZO samples, there is a single conduction mechanism, completely absent of any blocking grain boundary effects leading to a mobility increase.

Another energetically favourable process is the annihilation of the aluminium-zinc-vacancy (Al_{Zn}–V_{Zn}) complex which has been identified as one of the dominant defects in Al-containing ZnO, and has a crucial role in limiting the *n*-type doping efficiency. The formation of these complexes removes the Al donor level and makes the doping ineffective [42,43]. Thienprasert et al. [12] showed, using the X-ray absorption near edge structures (XANES) technique in conjunction with first-principles calculations, that Al energetically prefers to substitute onto the Zn site,

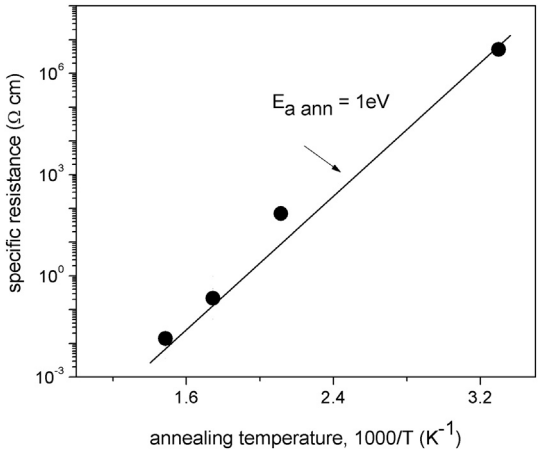

Fig. 12. DC resistivity of the AZO thin films at room temperature, as a function of the annealing temperature (obtained from Fig. 7). The straight line represents the activation energy (corresponding to the annealing) of 1 eV.

forming a donor Al_{Zn}, over being an interstitial, Al_i. On the other hand, the most probable intrinsic defects formed while doping with Al are zinc vacancies since their formation energy is relatively low [44]. Combining these two facts, the formation of Al_{Zn}–V_{Zn} complexes has a high probability resulting in a reduction of the carrier concentration and mobility in AZO samples. This explains their poor conductivity, despite the relatively high Al concentration. However, this calculation is valid for equilibrium processes, and may not be completely appropriate for magnetron sputtering. Nevertheless, the thermal treatment could activate the Al on substitutional Zn sites as a donor, since the dissociation energy of the Al_{Zn}–V_{Zn} complex, according to Ref. [42,12], is found to be 0.75 eV and 0.56 eV, respectively.

5. Conclusions

The effect of annealing in a hydrogen atmosphere on the structural, optical and electrical properties of AZO thin films, obtained by DC magnetron sputtering, was examined. After deposition, the samples were heated for one hour in a hydrogen atmosphere at temperatures of 200, 300 or 400 °C.

The structural investigation demonstrated that annealing reduces the strain in the material, and the volume of the crystal lattice decreases due to a decrease of the unit cell parameters. Also, the crystallite size grows from 9.7 nm for the as-deposited sample, to 17.2 nm for the sample heated at 400 °C. The changes in the crystal lattice parameters (GIXRD results) towards structural ordering could be a consequence of annihilation of point defects, where interstitial atoms recombine with vacancies or simply diffuse out on the crystal surface, as concluded from our PL measurements.

By measuring the optical properties, it was shown that heating increases the optical gap (from 2.85 eV to 3.07 eV) and nullifies defects related to interstitial atoms. The increase of the optical gap is consistent with the increase of conductivity, if the dominant contribution comes from the increase of the free carrier concentration since these electrons occupy the lowest energy levels in the conduction band.

This kind of annealing may change the conductivity of the AZO thin films by almost 9 orders of magnitude as a result of the increased mobility and concentration of free charge carriers due to the reduced number of defects and the activation of the dopants as shallow donors. In doing so, the most probable process is the diffusion of interstitial atoms, along with the annihilation of vacancies, and the passivation of defects at the grain boundaries.

Acknowledgments

This work has been supported by Croatian Science Foundation under the project IP-2014-09-9419.

References

[1] B. Weintraub, Z. Zhou, Y. Li, Y. Deng, Solution synthesis of one-dimensional ZnO nanomaterials and their applications, Nano 2 (2010) 1573–1587.
[2] X.W. Sun, J.Z. Huang, J.X. Wang, Z. Xu, A ZnO nanorod inorganic/organic heterostructure light-emitting diode emitting at 342 nm, Nano Lett. 8 (2008) 1219–1223.
[3] C.S. Rout, C.N.R. Rao, Electroluminescence and rectifying properties of heterojunction LEDs based on ZnO nanorods, Nanotechnology 19 (2008) 285203.
[4] J.M. Wu, Y.-R. Chen, Y.-H. Lin, Rapidly synthesized ZnO nanowires by ultraviolet decomposition process in ambient air for flexible photodetector, Nano 3 (2011) 1053–1058.
[5] H. Lu, L. Liao, J. Li, D. Wang, H. He, Q. Fu, L. Xu, Y. Tian, High surface-to-volume ratio ZnO microberets: low temperature synthesis, characterization, and photoluminescence, J. Phys. Chem. B 110 (2006) 23211–23214.
[6] K. Liu, M. Sakurai, M. Aono, ZnO-based ultraviolet photodetectors, Sensors 10 (2010) 8604–8634.
[7] K. Keis, C. Bauer, G. Boschloo, A. Hagfeldt, K. Westermark, H. Rensmo, H. Siegbahn, Nanostructured ZnO electrodes for dye-sensitized solar cell applications, J. Photochem. Photobiol., A 148 (2002) 57–64.
[8] A. Janotti, C.G. van de Walle, Fundamentals of zinc oxide as a semiconductor, Rep. Prog. Phys. 72 (2009) 126501.
[9] J.T. Thienprasert, S. Rujirawat, W. Klysubun, J.N. Duenow, T.J. Coutts, S.B. Zhang, D.C. Look, S. Limpijumnong, Compensation in Al-doped ZnO by Al-related acceptor complexes: synchrotron X-ray absorption spectroscopy and theory, Phys. Rev. Lett. 110 (2013) 055502.
[10] A.B. Djurišić, Y.H. Leung, Optical properties of ZnO nanostructures, Small 2 (2006) 944–961.
[11] T.S. Li, G. He, W.D. Li, B. Deng, M. Zhang, C.Y. Zheng, Z.Q. Sun, Microstructure optimization and optical properties modulation of sputtering-derived ZnO thin films, Sci. Adv. Mater. 6 (2014) 908–914.
[12] G. He, J. Liu, H. Chen, Y. Liu, Z. Sun, X. Chen, M. Liu, L. Zhang, Interface control and modification of band alignment and electrical properties of HfTiO/GaAs gate stacks by nitrogen incorporation, J. Mater. Chem. C 2 (27) (2014) 5299–5308.
[13] J.W. Zhang, G. He, L. Zhou, H.S. Chen, X.S. Chen, X.F. Chen, B. Deng, J.G. Lv, Z.Q. Sun, Microstructure optimization and optical and interfacial properties modulation of sputtering-derived HfO_2 thin films by TiO_2 incorporation, J. Alloys Compd. 611 (2014) 253–259.
[14] W.L. Dang, Y.Q. Fu, J.K. Luo, A.J. Flewitt, W.I. Milne, Deposition and characterization of sputtered ZnO films, Superlattice. Microst. 42 (2007) 89–93.
[15] S.S. Lin, J.L. Huang, P. Šajgalik, The properties of heavily Al-doped ZnO films before and after annealing in the different atmosphere, Surf. Coat. Technol. 185 (2004) 254–263.
[16] B.Y. Oh, M.C. Jeong, J.M. Myoung, Stabilization in electrical characteristics of hydrogen-annealed ZnO:Al films, Appl. Surf. Sci. 253 (2007) 7157.
[17] S.J. Baik, J.H. Jang, C.H. Lee, W.Y. Cho, K.S. Lim, Highly textured and conductive undoped ZnO film using hydrogen post-treatment, Appl. Phys. Lett. 70 (1997) 3516.
[18] H. Tong, Z. Deng, Z. Liu, C. Huang, J. Huang, H. Lan, C. Wang, Y. Cao, Effects of post-annealing on structural, optical and electrical properties of Al-doped ZnO thin films, Appl. Surf. Sci. 257 (2011) 4906–4911.
[19] A. Lausi, E. Busetto, M. Leoni, P. Scardi, The MCX project: a powder diffraction beamline at ELETTRA, Synchrotron Radiation in Natural Science 5 (2006) 5.
[20] K. Jurać, D. Gracin, I. Djerdj, A. Lausi, M. Čeh, D. Balzar, Structural analysis of amorphous-nanocrystalline silicon thin films by grazing incidence X-ray diffraction, Nucl. Instrum. Meth. B 284 (2012) 78–82.
[21] D. Gracin, A. Gajovic, K. Juraic, M. Ceh, Z. Remes, A. Poruba, M. Vanecek, Spectral response of amorphous–nano-crystalline silicon thin films, J. Non-Cryst. Solids 354 (2008) 2286–2290.
[22] A. Gajović, D. Gracin, I. Djerdj, N. Tomašić, K. Juraić, D.S. Su, Nanostructure of thin silicon films by combining HRTEM, XRD and Raman spectroscopy measurements and the implication to the optical properties, Appl. Surf. Sci. 254 (2008) 2748–2754.
[23] A. Moguš-Milanković, A. Šantić, S.T. Reis, K. Furić, D.E. Day, Studies of lead-iron phosphate glasses by Raman, Mossbauer and impedance spectroscopy, J. Non-Cryst. Solids 351 (2005) 3246–3258.
[24] D. Meljanac, N. Krstulović, K. Juraić, K. Salamon, H. Skenderović, Z. Siketić, S. Bernstorff, Z. Kregar, M. Plodinec, I. Šrut Rakič, D. Gracin, Influence of RF excitation during pulsed laser deposition in oxygen atmosphere on the structural properties and luminescence of nanocrystalline ZnO:Al thin films, J. Vac. Sci. Technol. A 34 (2016) 021514.
[25] E. Burstein, T.S. Moss, Anomalous optical absorption limit in InSb, Phys. Rev. 93 (1954) 632The interpretation of the properties of indium antimonide, Proc. Phys. Soc. Section B 67 (1954) 775.
[26] J. Tauc, R. Grigorovici, A. Vancu, Optical properties and electronic structure of amorphous germanium, Phys. Status Solidi B 15 (1966) 627–637.
[27] J. Sancho-Parramon, D. Gracin, M. Modreanu, A. Gajovic, Optical spectroscopy study of nc-Si-based p–i–n solar cells, Sol. Energy Mater. Sol. Cells 93 (2009) 1768–1772.
[28] H. Kaftelen, K. Ocakoglu, R. Thomann, S. Tu, S. Weber, E. Erdem, EPR and photoluminescence spectroscopy studies on the defect structure of ZnO nanocrystals, Phys. Rev. B 86 (2012) 014113.
[29] P.S. Xu, Y.M. Sun, C.S. Shi, F.Q. Xu, H.B. Pan, The electronic structure and spectral properties of ZnO and its defects, Nucl. Instrum. Methods Phys. Res., Sect. B 199 (2003) 286–290.
[30] D. Zhao, C. Andreazza, P. Andreazza, J. Ma, Y. Liu, D. Shen, Temperature-dependent growth mode and photoluminescence properties of ZnO nanostructures, Chem. Phys. Lett. 399 (2004) 522–526.
[31] X. Liu, X. Wu, H. Cao, R.P.H. Chang, Growth mechanism and properties of ZnO nanorods synthesized by plasma-enhanced chemical vapor deposition, J. Appl. Phys. 95 (2004) 3141.
[32] R.B.M. Cross, M.M. de Souza, E.M. Sankara Narayanan, A low temperature combination method for the production of ZnO nanowires, Nanotechnology 16 (2005) 2188–2192.
[33] W.M. Kwok, Y.H. Leung, A.B. Djurisic, W.K. Chan, D.L. Phillips, Time-resolved photoluminescence study of the stimulated emission in ZnO nanoneedles, Appl. Phys. Lett. 87 (2005) 093108.
[34] M.C. Jeong, B.Y. Oh, M.H. Ham, J.M. Myoung, Electroluminescence from ZnO nanowires in n-Zn O film/ZnO nanowire array/p-Ga N film heterojunction light-emitting diodes, Appl. Phys. Lett. 88 (2006) 202105.
[35] A. Šantić, A. Moguš-Milanković, Charge carrier dynamics in materials with disordered structures: a case study of iron phosphate glasses, Croat. Chem. Acta 85 (2012) 245–254.
[36] A. Moguš-Milanković, A. Šantić, V. Ličina, D.E. Day, Dielectric behavior and impedance spectroscopy of bismuth iron phosphate glasses, J. Non-Cryst. Solids 351 (2005) 3235–3245.
[37] C.H. Song, H.W. Choi, J.E. Kim, J.K. Lee, S.J. Kim, Y.S. Yang, Dielectric properties of $KNbGeO_5$ glass, J. Korean Phys. Soc. 46 (2005) 167.
[38] J. Jose, M. Abdul Khadar, Role of grain boundaries on the electrical conductivity of nanophase zinc oxide, Mater. Sci. Eng. A 304 (2001) 810–813.
[39] J. Jose, M.A. Khadar, Role of grain boundaries on the electrical properties of ZnO–ag nanocomposites: an impedance spectroscopic study, Acta Mater. 49 (2001) 729.

[40] P. Erhart, K. Albe, Diffusion of zinc vacancies and interstitials in zinc oxide, Appl. Phys. Lett. 88 (2006) 201918.
[41] M.D. McCluskey, Chapter eight-point defects in ZnO, Semiconductors and Semimetals 91 (2015) 279–313.
[42] K.M. Johansen, L. Vines, T.S. Bjørheim, R. Schifano, B.G. Svensson, Aluminum migration and intrinsic defect interaction in single-crystal zinc oxide, Phys. Rev. Applied 3 (2015) 024003.
[43] J.E. Stehr, K.M. Johansen, T.S. Bjørheim, L. Vines, B.G. Svensson, W.M. Chen, I.A. Buyanova, Zinc-vacancy–donor complex: a crucial compensating acceptor in ZnO, Phys. Rev. Applied 2 (2014) 021001.
[44] G. Luka, T.A. Krajewski, B.S. Witkowski, G. Wisz, I.S. Virt, E. Guziewicz, M. Godlewski, Aluminum-doped zinc oxide films grown by atomic layer deposition for transparent electrode applications, J. Mater. Sci. Mater. Electron. 22 (2011) 1810–1815.